

Total Opacity of Local Group Galaxies and Large Scale Structure behind the Galactic Bulge

Rosa A. González

Centro de Radioastronomía y Astrofísica, UNAM, Morelia, Mexico

Benne Holwerda

Kapteyn Institute, Groningen, The Netherlands

Laurent Loinard

Centro de Radioastronomía y Astrofísica, UNAM, Morelia, Mexico

Ronald J. Allen

Space Telescope Science Institute, Baltimore, MD, USA

Sébastien Muller

Academia Sinica Institute of Astronomy and Astrophysics, Taipei, Taiwan

Abstract. Recently, we have developed and calibrated the Synthetic Field Method to derive total extinction through disk galaxies. The method is based on the number counts and colors of distant background field galaxies that can be seen through the foreground object. Here, we investigate how large (10-m) and very large (20 to 30-m), diffraction-limited, optical and infrared telescopes in space would improve the detection of background galaxies behind Local Group objects, including the Galactic bulge. We find that, besides and perhaps more important than telescope size, a well-behaved, well-characterized PSF would facilitate in general the detection of faint objects in crowded fields, and greatly benefit several other important research areas, like the search for extrasolar planets, the study of quasar hosts and, most relevant for this meeting, the surveying of nearby large scale structure in the Zone of Avoidance, in particular behind the Galactic bulge.

1. Introduction

González et al. (1998) developed and calibrated the Synthetic Field Method (SFM) to derive the total extinction through disk galaxies. The method is based on the number counts and colors of distant background field galaxies that can be seen through the foreground object; it is the only method capable of determining total extinction without *a priori* assumptions about the dust properties or its spatial distribution. In principle, applying the SFM to the nearest galaxies, like M 31 and the Magellanic Clouds, could offer a unique opportunity to study the distribution of dust on small scales, to compare the distributions

of warm and cold dust, and to obtain the mass of molecular gas independently of the highly uncertain CO to H₂ conversion factor. Unfortunately, background galaxies cannot be easily identified through Local Group galaxies, even with the resolution provided today by the Hubble Space Telescope (*HST*; González et al. 2003). This paucity of detected background objects results in relatively large uncertainties on the determination of the opacities (0.8 mags and 1.3 mags, respectively, in the LMC and M 31; see Table 1).

In the case of M 31, each pixel in the WFPC2 images contains 50-100 stars, and the background galaxies cannot be seen because of the strong surface brightness fluctuations produced by nearly resolved stars. In the LMC, on the other hand, there is only about one star every 6 linear pixels, and the lack of detectable background galaxies is the effect of a “secondary” granularity, introduced by structure in the wings of the point-spread function (PSF). As it often happens, technological advances pose new problems, and going over the atmosphere has had the unintended consequence that we now have to worry more about the “beauty” of the PSF.

The work discussed below about simulated observations of the LMC and M 31 with diffraction-limited optical telescopes ≤ 10 -m has been published in an extended form before (González et al. 2003). The predictions for 20-m and 30-m telescopes, however, appear here in print for the first time. The section about the Galactic bulge is completely new.

2. M 31 and the LMC

2.1. Strategy

To quantify the effects of the granularity, we produced artificial stellar fields and measured their effect on the detectability of background galaxies. These simulations were all produced in the *V* passband, i.e., as if they had been obtained through the *HST* filters *F555W* or *F606W*. The simulations had several levels: first, we reproduced LMC and M 31 *HST* Wide Field Planetary Camera 2 (WFPC2) data, guided by published luminosity functions and/or the star counts of the data, and constrained by the mean and rms of the images. The second step was to simulate the change in resolution offered, first by the smaller pixels of the Advanced Camera for Surveys (ACS) on-board *HST*, then by increasingly bigger, diffraction-limited telescopes. This was achieved by changing the numbers of stars per pixel. Here, we did two subclasses of simulations. In one case, we used Gaussian PSFs and assumed that they were fully sampled. In the other, we used the Tiny Tim PSFs for the two ACS cameras. Since the PSF for the ACS High Resolution Camera (ACS-HR) is Nyquist-sampled in the visible, we used it to simulate the observations with larger telescopes. Finally, we added the HDF-N to every simulated stellar field, in order to assess the number of background galaxies that we can expect to see in the absence of extinction. When few HDF-N galaxies can be seen, it is impossible to know whether the paucity of real background galaxies is due to crowding or extinction.

Table 1. Error in opacity measurement (mags), 5.3 arcmin² FOV

Telescope size (m)	M 31 (2 hr exposure)		LMC (30 min exposure)	
	“Real” PSF	Gaussian PSF	“Real” PSF	Gaussian PSF
2.4 (WFPC2)	1.3		0.8	
0.8		1.2		0.7
1.1		1.0		0.6
2.4 (ACS-WFC)	0.9		0.6	
1.6		0.8		0.6
2.3		0.7		0.4
2.4 (ACS-HRC)	0.9		0.6	
3.	0.9		0.7	
3.2		0.6		0.3
4.5	0.8		0.6	
6.	0.8			
10.	0.8	0.5	0.5	0.2
20.	0.5	0.3	0.2	0.3
30.	0.5	0.3	0.3	0.3

Note. — Except for *HST* with WFPC2 and ACS-WFC, all telescopes are diffraction-limited. All Gaussian PSFs, and “real” PSFs of telescopes 2.4-m and larger are well sampled.

Figure 1 shows the galaxy counts in the M 31 simulations. The field of view of 5.3 arcmin^2 is equal to that of the combined three wide-field chips of the WFPC2. Changing the resolution of the telescope helps little, until the number of stars per pixel falls below about one, where a jump can clearly be seen. This jump corresponds to a change of regime when, with less than one star per pixel, one encounters a situation similar to that of the LMC and secondary granularity becomes strongly dominant. Indeed, the difference between Gaussian and realistic PSFs turns significant only then. Exposure time is never an issue with a realistic PSF; it only becomes important with a Gaussian PSF and for telescopes 10-m and larger.

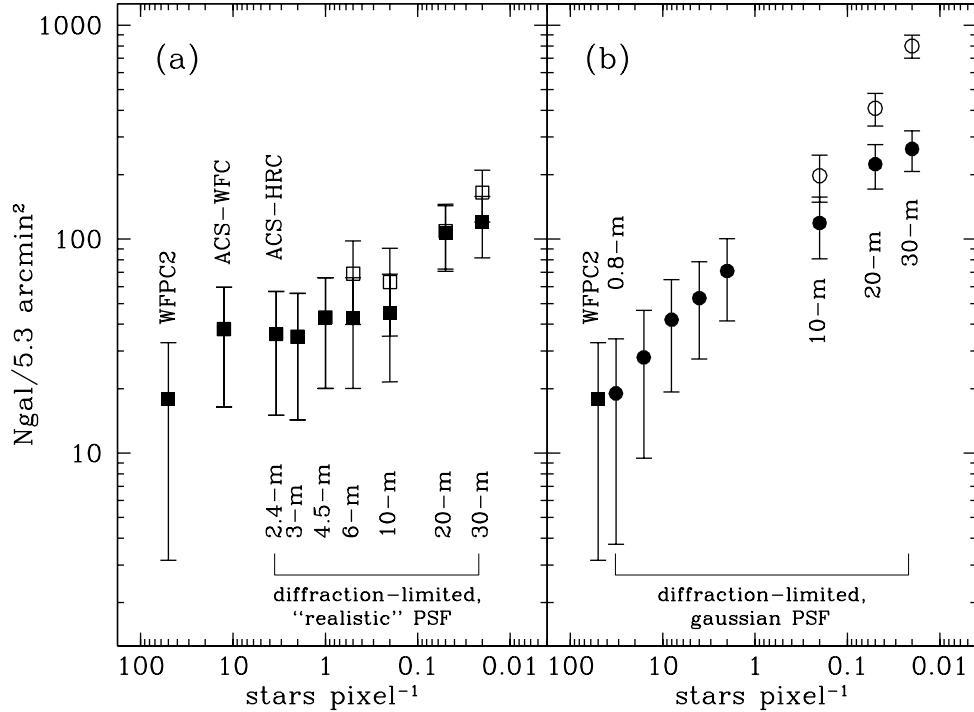


Figure 1. Galaxy counts in M 31 simulations. (a): “Realistic” Tiny Tim PSF. (b): Gaussian, fully sampled PSF (except for WFPC2 simulation). Open symbols: Noiseless data. Filled symbols: 2 hr exposures with HST. This time should be scaled by $(2.4/D)^2$ for each pointing with telescopes with different aperture D in meters; however, since the field-of-view will likely decrease also as D^{-2} , total exposure times should stay roughly constant. Error bars are 3.5 times Poisson, in order to account for field galaxy clustering.

Figure 2 displays galaxy counts in the LMC simulations. For “small” telescopes, this is the case where one would benefit most from both a Gaussian PSF and long exposure times. Very large telescopes, on the other hand, would image about one star every 50 linear pixels (i.e., mostly “empty” space). In those

circumstances, PSF would be inconsequential, and exposure time would become an important factor.

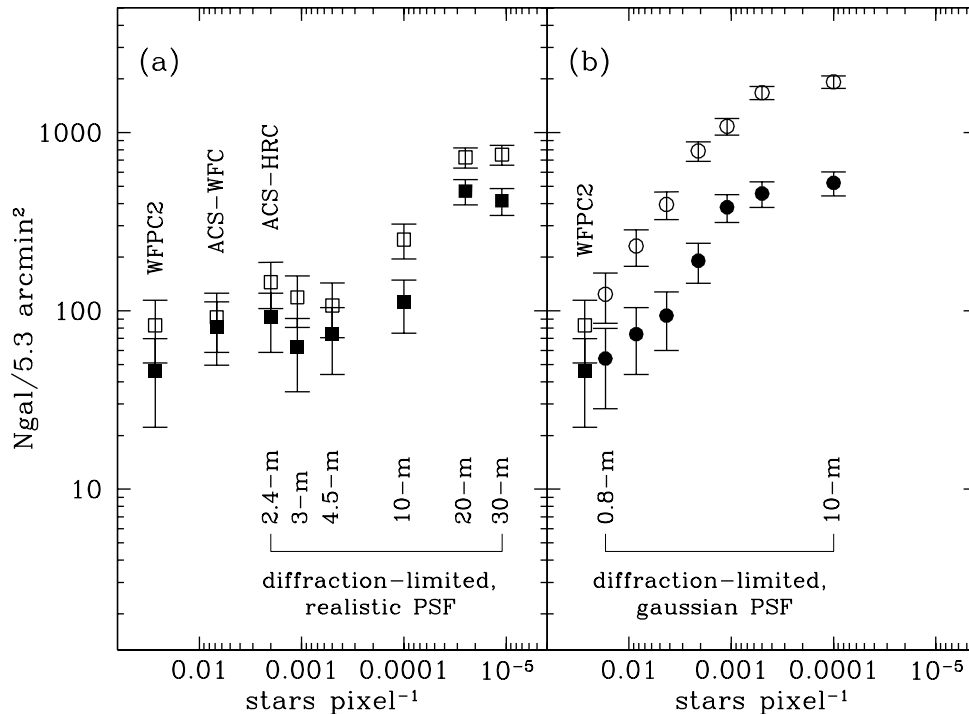


Figure 2. Galaxy counts in the LMC simulations. The field of view of 5.3 arcmin² is equal to that of the combined three wide-field chips of the WFPC2. (a): “Realistic” Tiny Tim PSF. (b): Gaussian, fully sampled PSF (except for WFPC2 simulation). Open symbols: Noiseless data. Filled symbols: 30 min exposures with *HST*; this time should be scaled by $(2.4/D)^2$ for telescopes with different aperture D in meters. Error bars are 3.5 times Poisson, in order to account for galaxy clustering.

2.2. The model

The behavior of background galaxy detection as a function of distance to the foreground galaxy and telescope size can be understood in a simple statistical way, especially in the case of a Gaussian PSF (for details, see González et al. 2003). Assuming that all foreground stars are identical, and have an intrinsic flux f_* (in photons sec⁻¹ received at the detector), a background galaxy will be detected with a signal-to-noise ratio equal to the quotient of the number of photons received from that background object ($f_{bg}t$) divided by the noise produced by Poisson fluctuations in both the stellar photons and the number n of foreground stars:

$$\left(\frac{S}{N}\right)_o = \frac{f_{bg}t}{t\sqrt{nf_*^2 + n^2f_*}} = \frac{f_{bg}}{\sqrt{nf_*^2 + n^2f_*}} \quad (1)$$

When telescope resolution is improved and pixels are made L times smaller (on a side), signal-to-noise ratio becomes:

$$\left(\frac{S}{N}\right)_n = \frac{L f_{bg}}{\sqrt{L^2 n f_*^2 + n^2 f_*}} \quad (2)$$

If the same foreground stellar population is pushed d times farther away, the signal-to-noise ratio results in:

$$\left(\frac{S}{N}\right)_d = \frac{L f_{bg}}{\sqrt{\frac{L^2 n f_*^2}{d^2} + n^2 f_* d^2}}. \quad (3)$$

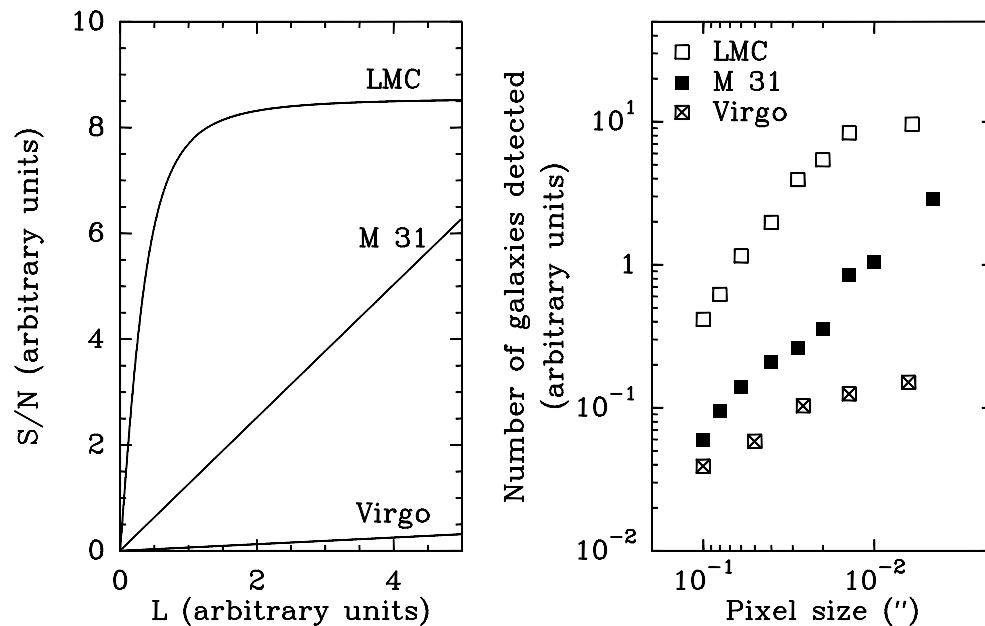


Figure 3. Comparison of the behavior of eq. (3) (*left*) with the number of background galaxies detected through the LMC, M 31, and Virgo (*right*); an arbitrary constant has been added to the logarithm of the number of background galaxies seen through each object to facilitate the comparison of the data with the model.

The behavior of this expression as a function of pixel size (set by L) for the same stellar population at three different distances d is shown on the left panel of Figure 3. The value of f_* , the average stellar flux, and n , the number of stars per pixel, have been chosen to reproduce (although with arbitrary units) the conditions in the LMC; we further mimic the conditions found in M 31 and Virgo by changing only d , the relative distance. The qualitative agreement between the left and right panels of Figure 3 is remarkable, especially given the extremely simple model we have adopted for the noise.

3. Application to the Galactic bulge

The Galactic bulge occupies approximately one thirty-seventh of the sky, or the area of more than 5000 Suns! It constitutes almost one-third of the Zone of Avoidance. Although quantifying the extinction suffered by galaxies seen through the bulge has interest, it is potentially much more important to characterize the distribution of nearby galaxies behind the bulge. Except at very low latitudes ($b \lesssim 2^\circ$), the main obstacle to finding galaxies in this region of the sky is stellar crowding, more than dust extinction (Kraan-Korteweg & Lahav 2000; Kraan-Korteweg 2004, personal communication). Going to the near-IR to try to circumvent extinction only makes stellar crowding worse, since the old and metal rich population of the bulge emits strongly in this spectral region.

Short of doing simulations to try to quantify background galaxy detection rates behind the bulge in the near-IR, we have performed two little exercises. First, we notice (Tully 2004, personal communication) that the galaxy count-rate per interval of $\sin |b|$ in the Two Micron All-Sky Survey (2MASS) is flat up to $|b| \sim 13^\circ$ and then decreases steadily; almost no galaxies are seen at latitudes lower than $|b| \sim 1^\circ$. On the other hand, in the K -band, the surface brightness of the bulge is 100 times larger at $|b| \sim 1^\circ$ than at 13° (Kent, Dame, & Fazio 1991). This means that, in principle and in the absence of extinction, with a linear resolution 10 times better than that of 2MASS –which would allow us to image one hundred times fewer foreground bulge stars per pixel–, it would be possible to see as many background galaxies at $b \sim 1^\circ$ as can be detected at 13° .

The pixels of the released images of 2MASS are $1''$, and we have measured an average FWHM of $\sim 3''$. The resolution of the *HST* NICMOS Camera 2 (NIC2), with a pixel scale of $0''.075 \text{ pixel}^{-1}$, is already in the right ballpark; the problem is that the NIC2 field-of-view is very small ($19'' \times 19''$) and, of course, that the PSF is not Gaussian (see, for example, Krist et al. 1998).

The other exercise consists in the application of our toy model, only this time changing the “stellar population,” that is, the brightness of the average star and the stellar density. Stellar population synthesis models (Bruzual & Charlot 2003) show that $1 M_\odot$ of a population with solar metallicity and 10^{10} yr (i.e., like that of the bulge) has an absolute K mag $M_K \sim 3.7$. On the other hand, the LMC population that we have used as a template for our little model in §2.2. has an age of about 2 Gyr and $Z = 0.004$ (Elson, Gilmore, & Santiago 1997). According to Bruzual & Charlot (2003), $1 M_\odot$ of this population has $M_K \sim 2.7$, i.e., it is 1 mag brighter at K than the bulge population. The template LMC population has a surface brightness $\mu_K \sim 19.5$, while the Milky Way bulge has $\mu_K \sim 15$ at $|b| \sim 0 - 1^\circ$, and ~ 15.5 at $|b| \sim 4^\circ$. For our toy model, what all this means is that the old and metal rich population, which is intrinsically 1 mag fainter per solar mass than that of the LMC disk, produces a bulge surface brightness that is between 4 and 4.5 mag brighter. Consequently, the stellar density of the bulge must be 63 times and 158 times higher than that of the LMC disk at, respectively, $|b| \sim 4^\circ$ and $|b| \sim 0 - 1^\circ$. Figure 4 shows the change of background galaxy detection rate with resolution (again with units that are arbitrary, and different from those used in Figure 3) for the bulge stellar population, at these two different Galactic latitudes and in the near-IR. The population is set at one-sixth the distance to the LMC; it is assumed to be the same at both latitudes, except for the stellar density, and it is characterized

by an average brightness of a single star that is 40% of the one used in §2.2.. Predictably, the curve for $|b| \sim 4^\circ$ not only reaches higher, but also –although it is hard to notice– rises faster. The extremely fast upsurge of the detection rate in both cases, however, confirms that a telescope in space as small as the Hubble could do the job, provided it had adequate optics and a large field of view. Also, by comparison with the simulations of the LMC and M 31, we could expect satisfactory results with a “realistic,” non-optimized, PSF already with a 10-m class telescope in space.

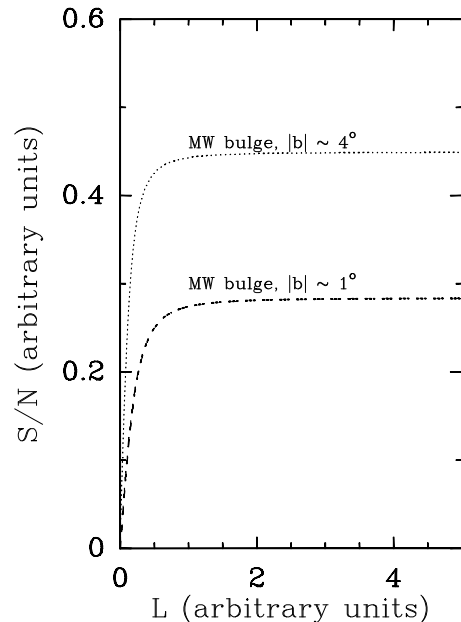


Figure 4. Behavior of eq. (3) for bulge parameters. *Dashed line*: $|b| \sim 1^\circ$; *dotted line*: $|b| \sim 4^\circ$. The distance of the foreground population is 1/6 of that to the LMC. To mimic an old and metal-rich stellar population, as well as observations in the near-IR, the average flux of an individual star is taken to be 40% of the one used in Figure 3. Always comparing with the LMC disk, the stellar density is, respectively, 158 and 63 times higher.

4. Conclusions

We have investigated how large and very large, diffraction-limited, optical and infrared telescopes in space would improve the detection of background galaxies behind Local Group objects, including the Galactic bulge. For example, with a 20-m optical telescope, the total extinction through the LMC could be determined with an error of 0.2 mags in a field of view of 5.3 arcmin^2 , in about 30 min total exposure time, independently of the quality of the PSF. Likewise, the number of galaxies seen behind the Galactic bulge should increase significantly, in spite of the high extinction in the midplane, with a 10-m infrared telescope; important strides could be made behind the bulge even with a smaller telescope,

provided the PSF were close to Gaussian. Indeed, probably more important than a large aperture, a well-behaved, well-characterized PSF would facilitate in general the detection of faint objects in crowded fields, and greatly benefit several important research areas, like the determination of total extinction in Local Group objects, the search for extrasolar planets, the study of quasar hosts and, most relevant for this meeting, the surveying of nearby large scale structure in the Zone of Avoidance, in particular behind the Galactic bulge.

References

- Bruzual, G. & Charlot, S. 2003, MNRAS, 344, 1000
Elson, R. A. W., Gilmore, G. F., & Santiago, B. X. 1997, MNRAS, 289, 157
González, R. A., Allen, R. J., Dirsch, B., Ferguson, H. C., Calzetti, D., & Panagia, N. 1998, ApJ, 506, 152
González, R. A., Loinard, L., Allen, R. J., & Muller, S. 2003, AJ, 125, 1182
Kent, S. M., Dame, T. M., & Fazio, G. 1991, ApJ, 378, 131
Kraan-Korteweg, R. C. & Lahav, O. 2000, A&A Rev., 10, 211
Krist, J. E., Golimowski, D. A., Schroeder, D. J., & Henry, T. J. 1998, PASP, 110, 1046